Design and optimization of an ultra-broadband six-mode multiplexer based on adiabatic waveguide branches forming photonic lantern

Quandong Huang
School of Information Engineering and Guangdong Provincial Key Laboratory of Information Photonics Technology
Guangdong University of Technology
Guangzhou, China
E-mail: qdhuang@gdut.edu.cn

Kang Li
School of Physics & Optoelectronic Engineering
Guangdong University of Technology
Guangzhou, China

Lixi Zhong
School of Information Engineering and Guangdong Provincial Key Laboratory of Information Photonics Technology
Guangdong University of Technology
Guangzhou, China

Jiancai Xue
School of Physics & Optoelectronic Engineering
Guangdong University of Technology
Guangzhou, China

Xinyong Dong
School of Information Engineering and Guangdong Provincial Key Laboratory of Information Photonics Technology
Guangdong University of Technology
Guangzhou, China

Ou Xu
School of Information Engineering and Guangdong Provincial Key Laboratory of Information Photonics Technology
Guangdong University of Technology
Guangzhou, China
E-mail: xuou@gdut.edu.cn

***Abstract*—We design and optimize an ultra-broadband mode multiplexer formed by photonic lantern that composed with adiabatic waveguide branches, which serves to spatially separate and combine the six modes over the C+L band and beyond.**

Keywords—optical waveguide, mode multiplexing, photonic lantern

I. Introduction

With the explosive large-capacity communications demanded, growing data traffic becomes a challenge in the optical communication network. Mode division multiplexing (MDM) technology is a compromised way to relieve the heavy optical communication data load [1], [2]. Mode multiplexer is a key component in MDM systems. And in the future, MDM systems should cover wider wavelength range from the O-band to U-band as estimated [3]. Many arts are contributed to spatially (de)multiplex the modes by the use of adiabatic waveguide structures such as the reported directional couplers [4], fiber photonic lantern [5], and waveguide branches [6]. The devices formed by waveguide branches have the merits of compact dimension and flexible design. However, the reported waveguide branches forming photonic lantern demonstrates for (de)multiplexing four waveguide modes, which is the lack of systematical analysis of the mode evolution mechanism, error analysis, and the challenges when more waveguide modes (such as six waveguide modes) are evolved. The device should cover six waveguide modes to be consistent with the fiber modes, and as a result, to fill the gap between waveguide and fiber devices.

In this paper, we present an ultra-broadband six-mode multiplexer formed by photonic lantern and analyze the detailed design of the device. The optimization scheme and the tolerances of the device is carried out as well for supporting the fabrication process.

II. Operation Principle and Device Design

A schematic diagram of the proposed photonic lantern is shown in Fig. 1, where a few-mode core (FMC) is divided into six parts with different areas and the divided six adiabatic waveguide branches are used together to form the layouts of the photonic lantern. Six waveguide modes (the E_{11}, E_{21}, E_{12}, E_{22}, E_{31} and E_{13} modes) are launched into the FMC from the MUX end with the corresponding output (C1, C2, C3, C4, C5 and C6) from the DeMUX end, and vice versus.

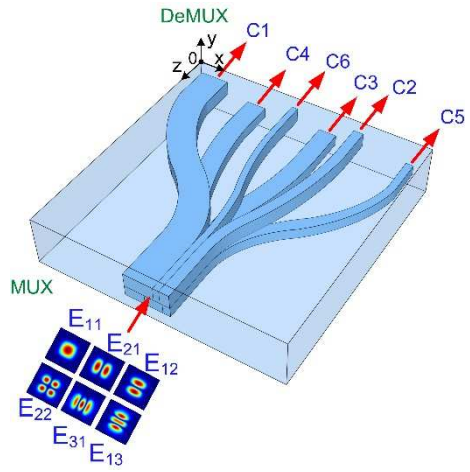

Fig. 1. Schematic diagram of the proposed photonic lantern, which is formed by six adiabatic waveguide branches and a combined FMC.

To study the mode evolution, the E_{11} modes are launched from the single-mode core (SMC), which is propagating along the adiabatic waveguide branches and output at the FMC port finally, where the launched E_{11} modes are converted into the E_{11}, E_{21}, E_{12}, E_{22}, E_{31} and E_{13} modes in the FMC. The core areas are of different sizes, so the divisions of FMC into six parts should meet the rule of the mode evolution. As shown in Fig. 2, we study the division of the FMC by using the finite element method. The proportion of the divided FMC has many compositions of core width and core height, where the composited core dimensions can achieve the function of the mode evolution from the E_{11} modes to the modes supported by the FMC. The variations of the effective indices along the propagation direction (z-direction) are shown in Fig. 3. By knowing the effective indices at the input and output ports, we can design the division of the FMC accordingly. As shown in

Fig. 4, by knowing the effective indices of the FMC, the division of the FMC can be systematically analyzed by calculating the mode dispersion against the core width with the core height fixed. When the FMC height is fixed at 12.4 μm, the effective indices increase with the FMC width increases. And if we fixed the FMC width at 13 μm, the division of the FMC depends on the two-layer core dimensions, which are the upper core-height and the lower core-height. Here for example, when the upper core-height are fixed at 8.4 μm, the lower layer core-height are also fixed at 4 μm. As a result, the sizes of all the SMCs are fixed. The device operating length is estimated to be about 5.5 mm.

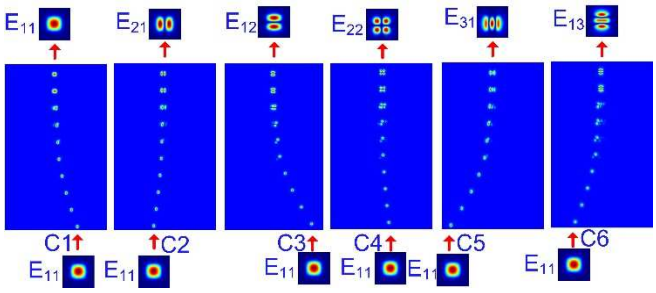

Fig. 2. Divisions of the FMC into six parts to achieve the mode evolution from the fundamental modes to the corresponding high-order modes.

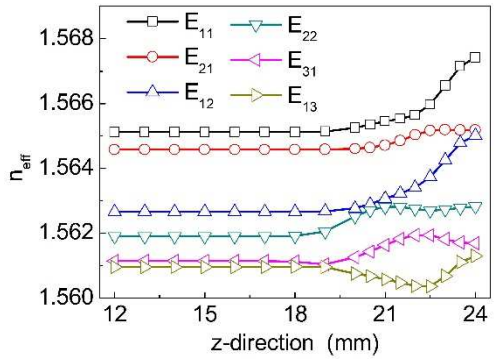

Fig. 3. Effective indices of the modes with the mode evolution from the fundamental modes to the corresponding high-order modes.

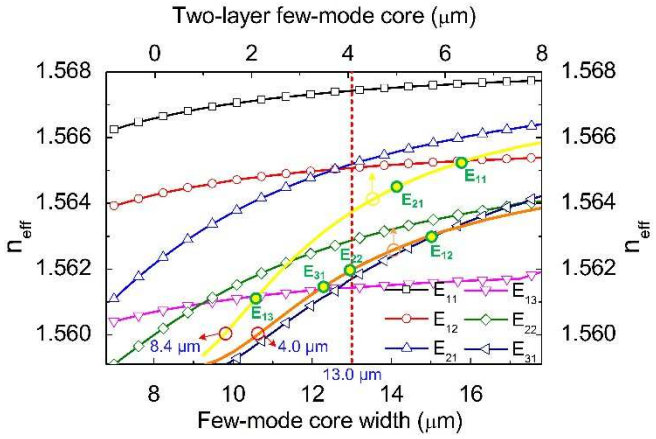

Fig. 4. Dispersion of the modes of the FMC against the core width (x-bottom, y-left axis); Dispersion of the fundamental mode of the upper cores and lower cores against the core width (x-top, y-right axis).

According to the theoretic studies above, the FMC with a core height of 12.4 μm and width of 13.0 μm is divided into six parts. As shown in Fig. 5, the upper layer cores have the same core height of 8.4 μm, C1, C6 and C2 that corresponding to the E_{11}, E_{13} and E_{21} modes in the FMC are with the core width of 6.1 μm, 2.1 μm and 4.8 μm, respectively, according to the analysis in Fig. 4. Similarly, the lower layer cores have the same core height of 4.0 μm, C4, C3 and C5 that corresponding to the E_{22}, E_{12} and E_{31} modes in the FMC are with the core width of 3.9 μm, 5.6 μm and 3.5 μm, respectively.

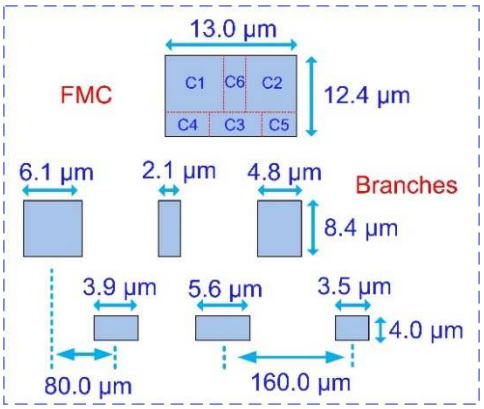

Fig. 5. One set of the obtained optional design parameters according to the calculations of the effective indices and the mode evolution.

III. Results and Discussion

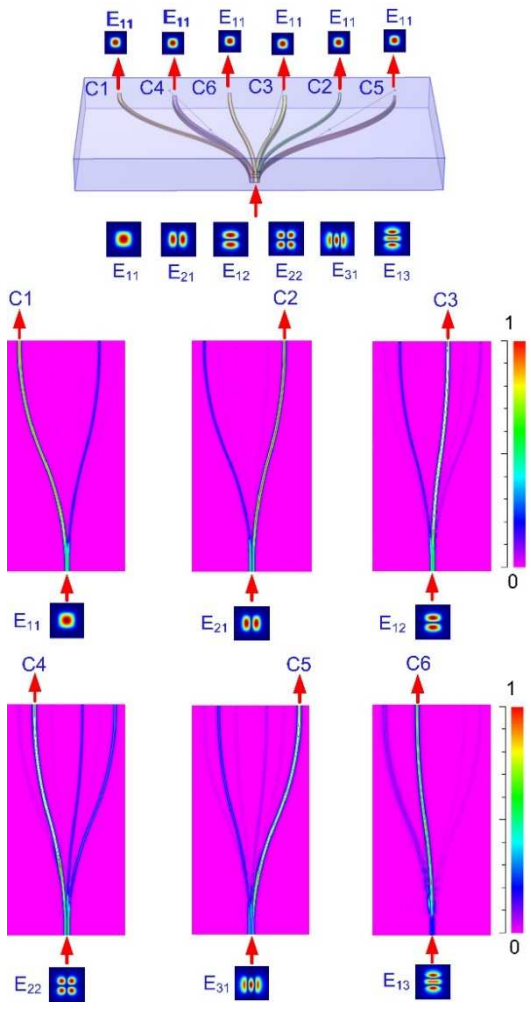

Fig. 6. Mode propagation path with the modes launched into the FMC, and output from the corresponding ports.

This work was supported by the National Natural Science Foundation of China, under Project 62205067, 62005052.

We follow the parameters obtained from the above theoretic analysis to build up the model for the simulation. As shown in Fig. 6, we use beam propagation method based commercial software (Rsoft) to prove the theory study. When the E_{11} mode is launched into the FMC of the photonic lantern, the power of the mode will output from C1 at the DeMUX end, where the powers output from the other ports are defined as crosstalks. Similarly, when the E_{21}, E_{12}, E_{22}, E_{31} and E_{13} modes are launched into the FMC, the power of the corresponding mode will output from C2, C3, C4, C5 and C6, respectively. The segments of the divided core parameters that affect the device performances will be analyzed in the follow section.

First, the variation of the two segments of the core heights is studied, i.e., the lower core-height decreases and the upper core-height increase with a total core height keeping as a constant of 12.4 μm. The detailed analysis is shown in Fig. 7, where the x-axis represents the variation of the lower layer cores' height (C4, C3 and C5) and the cores' height for the upper layer cores (C1, C6 and C2) are changed accordingly with FMC height keeping as a constant. The crosstalks of the E_{22} mode to the E_{12} mode that defined as $CT_{22\text{-}12}$, and similarly, $CT_{12\text{-}22}$, $CT_{31\text{-}13}$ and $CT_{22\text{-}13}$ increase with the lower layer cores' height decreasing. The $CT_{31\text{-}22}$ and $CT_{22\text{-}31}$ increase with the lower layer cores' height increasing. The other crosstalks show no significant changes.

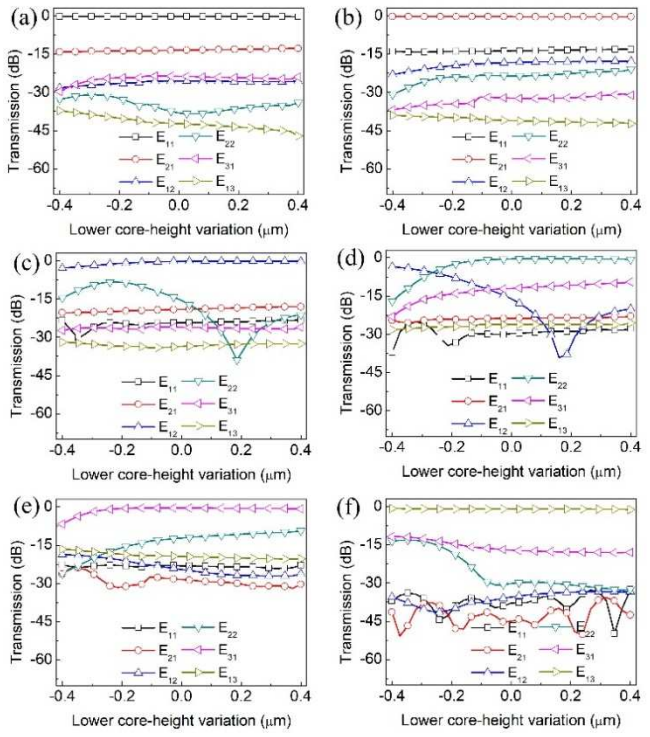

Fig. 7. Transmission spectra of the modes against the lower core-height variations with the FMC height keeping at a constant of 12.4 μm.

Then we used optimized design dimensions with the lower core-height of 4 μm and upper core-height of 8.4 μm to further analyze the core widths' variation that affect the device's performances. For the lower cores, we fixed the width of the central core (C3) at 5.6 μm, and change the core width of C4 and C5 simultaneously with the FMC width fixing at 13 μm, noted that the width variation of the C3 width shows little effect on the performances of the other modes of the device. The $CT_{31\text{-}22}$ and $CT_{22\text{-}31}$ increase when the C4 width decreases with the C3 width fixed, where the C5 width increases accordingly with the FMC width fixed at a constant of 13 μm. The $CT_{22\text{-}12}$ and $CT_{12\text{-}22}$ increase when the C4 width increases with the C3 width fixed, where the C5 width decreases accordingly. The other crosstalks show no significant changes.

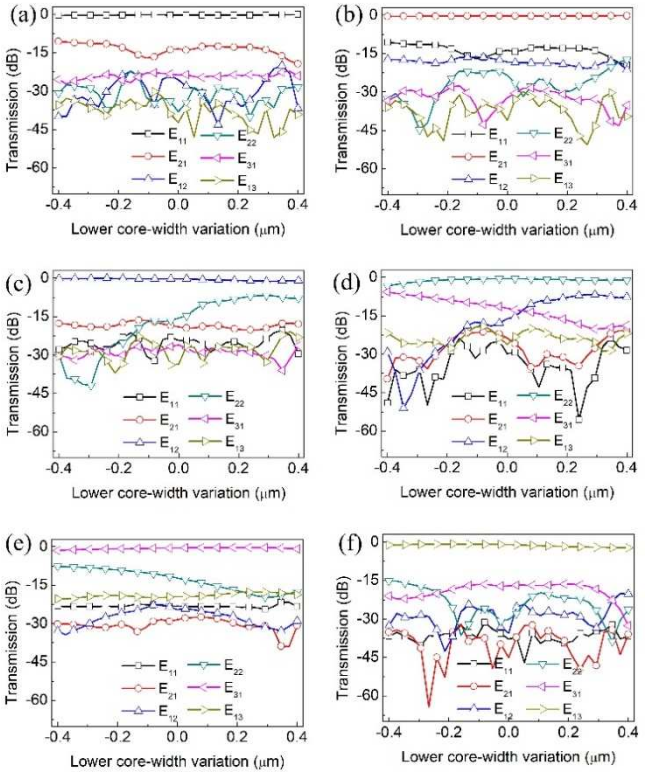

Fig. 8. Transmission spectra of the modes against the lower core-width variations with the FMC width keeping at a constant of 13.0 μm.

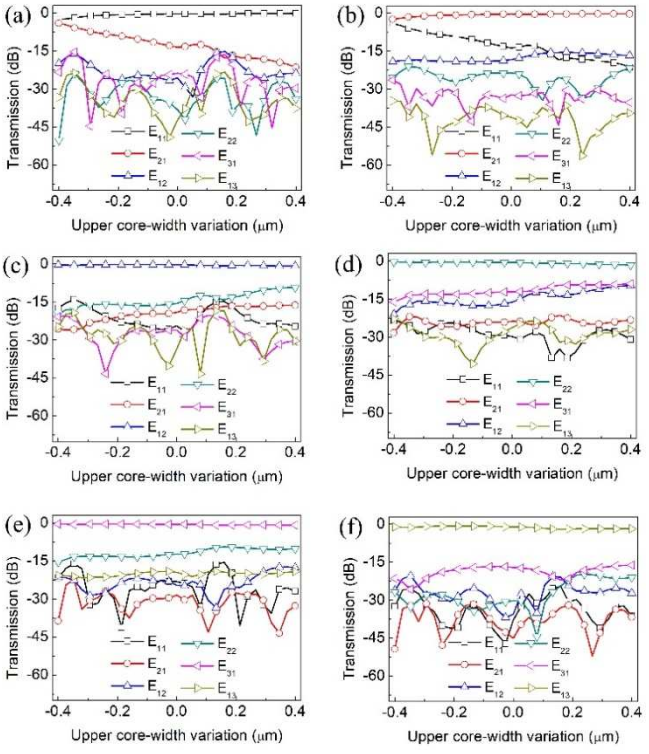

Fig. 9. Transmission spectra of the modes against the upper core-width variations with the FMC width keeping at a constant of 13.0 μm.

Similarly, for the upper cores, we fixed the width of the central core (C6) at 2.1 μm, and change the core width of C1 and C2 simultaneously with the FMC width fixing at 13 μm. noted that the width of C3 is the least flexible parameter of the device, which should be well cheat in the design due to the radiation loss that occurs during the E_{11}- E_{13} mode conversion. The $CT_{21\text{-}11}$ and $CT_{11\text{-}21}$ increase when the C1 width decreases with the C6 width fixed, where the C2 width increases accordingly with the FMC width fixed at a constant of 13 μm. The $CT_{22\text{-}21}$, $CT_{31\text{-}22}$, $CT_{12\text{-}22}$ and $CT_{22\text{-}31}$ increase when the C1 width increases with the C6 width fixed, where the C2 width decreases accordingly. The other crosstalks show no significant changes.

Finally, we study the transmission spectra against the wavelength for the C+L band. By scanning the wavelength, we get the powers from the six output ports at the DeMUX end with the E_{11}, E_{21}, E_{12}, E_{22}, E_{31} and E_{13} modes launched into the FMC at MUX end. The maximum insertion losses of the E_{11}, E_{21}, E_{12}, E_{22}, E_{31} and E_{13} modes are about 0.27 dB, 0.33 dB, 0.31 dB, 0.60 dB, 0.67 dB and 1.52 dB, respectively. The crosstalks of the E_{11}, E_{21}, E_{12}, E_{22}, E_{31} and E_{13} modes to the other mode channels are lower than −13.04 dB, −13.19 dB, −13.67 dB, −10.94 dB, −11.10 dB and −13.90 dB, respectively, over the C+L band. The proposed device is insensitive to the state of polarization.

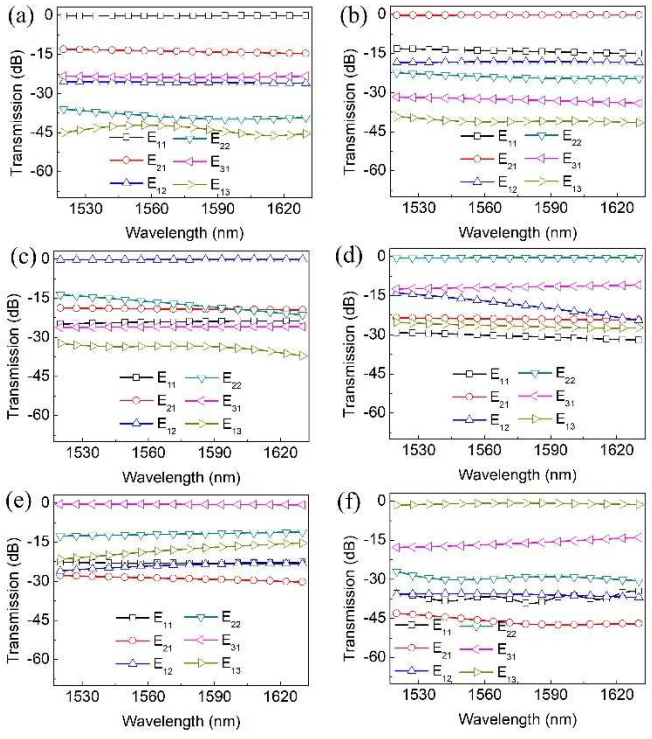

Fig. 10. Transmission spectra of the modes against the operation wavelength.

IV. Conclusion

We propose an ultra-broadband mode multiplexer that is composed of photonic lantern, which shows the insertion loss lower than 1.52 dB and modal crosstalks lower than −10.94 dB. For the reality application, such kind of device based on photonic lantern, however, has to fabricate by high precise fabrication micro fabrication system, such as two photon polymerization (2PP) technique-based 3D printing, to ensure the requirement of the device dimensions [7]-[9], where the fabrication resolution can reach 120 nanometers. The designed device can play an important role in mode manipulating area in a mode division multiplexing system where ultra-broadband operation wavelength is required or all-optical photonic chip for multi-input multi-output (MIMO) signal processing.

Acknowledgment

This work was supported by the National Natural Science Foundation of China, under Project 62205067, 62005052. The authors would like to thanks the undergraduate students (Mr. Q. Luo, Mr. H. Guo, Miss S. Jiang and Miss Y. Wu) to participate the extracurricular scientific research via this project.

References

[1] L. Zhang, J. Chen, E. Agrell, R. Lin and L. Wosinska, "Enabling Technologies for Optical Data Center Networks: Spatial Division Multiplexing," *J. Lightw. Technol.,* vol. 38, no. 1, pp. 18-30, Jan. 2020.

[2] B. J. Puttnam, G. Rademacher, and R. S. Luís, "Space-division multiplexing for optical fiber communications," Optica vol. 8, no. 9, pp. 1186-1203, Sep. 2021.

[3] B. Paredes, Z. Mohammed, J. Villegas, and M. Rasras, "Dual-Band (O & C-Bands) Two-Mode Multiplexer on the SOI Platform," IEEE Photonics J. vol. 13, no. 3, Art. 6600309, Jun. 2021.

[4] Q. Huang, J. Zhang, L. Zhong, Z. Zheng, J. Li, and O. Xu, "Three-dimensional mode multiplexer based on adiabatic-tapered waveguides forming vertical directional couplers over C+L band and beyond," Opt. Lett., vol.48, no. 4, pp. 1044-1047, Feb. 2023.

[5] A. M. Velazquez-Benitez, J. C. Alvarado, G. Lopez-Galmiche, J. E. Antonio-Lopez, J. Hernández-Cordero, J. Sanchez-Mondragon, P. Sillard, C. M. Okonkwo, and R. Amezcua-Correa, "Six mode selective fiber optic spatial multiplexer," Opt. Lett., vol.40, no. 8, pp. 1663-1666, Apr. 2015.

[6] Y. Wu and K. S. Chiang, "Ultra-broadband mode multiplexers based on three-dimensional asymmetric waveguide branches," Opt. Lett., vol. 42, no. 3, pp. 407–410, Feb. 2017.

[7] S. Kawata, H.-B. Sun, T. Tanaka, and K. Takada, "Finer features for functional microdevices," Nature, vol. 412, pp. 697–698, Aug. 2001.

[8] J. Linas, M. Dovilė, K. Gabrielius and P. Vytautas, "Femtosecond lasers: the ultimate tool for high-precision 3D manufacturing," Adv. Opt. Technol., vol. 8, no. 3-4, pp. 241-251, May 2019.

[9] A. Bertoncini and C. Liberale, "3D printed waveguides based on photonic crystal fiber designs for complex fiber-end photonic devices," Optica, vol. 7, no. 11, pp.1487–1494, Nov. 2020.